Histol Histopathol (2007) 22: 1309-1326

http://www.hh.um.es

Histology and Histopathology

Cellular and Molecular Biology

Standardization of an orthotopic mouse brain tumor model following transplantation of CT-2A astrocytoma cells

R. Martínez-Murillo and A. Martínez

Department of Cellular, Molecular, and Developmental Neurobiology, Instituto Cajal, Madrid, Spain

Summary. Animal models of glial-derived neoplasms are needed to study the biological mechanisms of glioma tumorigenesis and those that sustain the disease state. With the aim to develop and characterize a suitable in vivo experimental mouse model for infiltrating astrocytoma, with predictable and reproducible growth patterns that recapitulate human astrocytoma, this study was undertaken to analyze the long-term course of a syngeneic orthotopically implanted CT-2A mouse astrocytoma in C57BL/6J mice. Intracranial injection of CT-2A cells into caudate-putamen resulted in development of an aggressive tumor showing typical features of human glioblastoma multiforme, sharing close histological, immunohistochemical, proliferative, and metabolic profiles. To simulate metastatic disease to the brain, CT-2A cells were injected through the internal carotid artery. Tumors identical to those obtained by intracranial injection were obtained. Finally, CT-2A cells were re-isolated from experimental brain tumors and transcranially re-injected into the caudate-putamen of healthy mice. These cells generated new tumors that were indistinguishable from the initial ones, suggesting in vivo self-renewal of tumor cells. Small-animal models are essential for testing novel biological therapies directed against relevant molecular targets. In a preliminary study, experimental CT-2A tumors were chronically treated with the small molecule 77427, a gastrin-releasing peptide (GRP) blocker compound that inhibits angiogenesis. Treated animals developed significantly smaller tumors than controls, suggesting an antitumor action for 77427 in glioblastomas. We conclude that the orthotopic CT-2A tumor model, as described herein, is appropriate to explore the mechanisms of glioma development and for preclinical trials of promising drugs.

Offprint requests to: Alfredo Martinez, Department of Cellular, Molecular, and Developmental Neurobiology, Instituto Cajal, Avda. Doctor Arce 37, 28002 Madrid, Spain. e-mail: amartinez@cajal.csic.es

Key words: Astrocytoma, Animal model, Antiangiogenic treatment, Metastasis, Magnetic resonance imaging (MRI)

Introduction

Infiltrating gliomas (astrocytomas, glioblastomas, mixed gliomas, and oligodendrogliomas) represent the most common type of primary brain tumor (DeAngelis, 2001; Deorah et al., 2006), with an incidence rate of 5.9 per 100,000 persons-years in the United States according to the Central Brain Tumor Registry of the United States (www.cbtrus.org). Approximately 18,000 people in the United States are diagnosed annually with primary malignant brain tumors and approximately 13,000 people die from this disease annually (CBTRUS, 2005). Even though primary brain tumors are rare, accounting for merely 2-5% of all malignancies, they are, after stroke, a frequent cause of death from neurological disorders due to their remarkable resistance to available treatments. Neoplasms of the central nervous system (CNS) are, after leukaemia, the second cause of death due to cancer in children (Kaiser, 1999; McKinley et al., 2000). The highly infiltrative growth of malignant brain tumors and difficulties for drug penetration through the blood-brain barrier and the neural parenchyma determine a limited number of therapeutic options. Hence, there is a crucial need for new and better therapeutic strategies for brain tumors. The development of specific anti-cancer treatments requires a good understanding of the initiation and progression process of gliomas. Recently, specific brain tumor stem cells, named glioma stem cells, have been identified (Vescovi et al., 2006), although there is still discussion on whether these cells cause glioma initiation and progression or are the result of such processes (Fan et al., 2006).

Among the primary tumors found in the CNS, astrocytic neoplasms are by far the most common type.

Despite tremendous technical improvements in neuroimaging and neurosurgery, the morbidity and mortality caused by this malignancy is highly significant and the incidence of brain cancer is increasing in both children and the elderly (McKinley et al., 2000). Human astrocytomas are well-differentiated tumors that grow slowly and display an intrinsic tendency for diffuse infiltration of the neighboring brain structures. They habitually recur and naturally progress, according to the classification of the World Health Organization (WHO), from a lower-grade (WHO grade I), passing through a medium grade (WHO grade II) to a high-grade malignancy known as anaplastic astrocytoma (WHO grade III). The highest grade, glioblastoma multiforme (GBM) is the most malignant infiltrative astrocytoma and one of the most lethal of all cancers (WHO grade IV) (Kleihues and Ohgaki, 1997; Kleihues et al., 2002). Progression through this scale is responsible for the majority of patient mortality, providing also the rationale for early detection.

Understanding the tumor–host interactions represents an attractive objective for cancer therapy. In the CNS, tumors elicit a response from their host which includes, among others, angiogenesis. Angiogenesis is a complex physiological process involving a number of tightly controlled sequential events that occurs under normal and pathological conditions (Kaur et al., 2004). Tumor angiogenesis is a major independent prognostic factor since it is a key process in tumor growth and metastasis (Folkman, 1971; Jung et al., 2006; Kalluri and Zeisberg, 2006). Since all solid tumors are neovascularized by the time they are detected and in the absence of an adequate vasculature, tumor cells become necrotic and/or apoptotic (Holmgren et al., 1995), understanding the regulation of tumor angiogenesis has become one of the most exciting new developments in anticancer therapy (Gasparini et al., 2005). Microvascular proliferation is a key feature in glioma grading, separating low-grade primary tumors from malignant gliomas depending on the number of vessels per microscopic field (Wesseling et al., 1998). A number of angiogenesis inhibition strategies have been proposed as anticancer therapies (Brown and Wilson, 2004; Gasparini et al., 2005). In physiological states, angiogenesis depends on a strictly regulated equilibrium between stimulatory and inhibitory angiogenic factors (Folkman, 1992). In neoplasia, the angiogenic balance is tipped in favor of new vessel growth (Hanahan and Folkman, 1996). The onset of angiogenesis in cancer is under investigation and appears to involve down-regulation of endogenous angiogenesis inhibitors and the implication of intracellular pathways required for embryonic vascular development (Patel et al., 2005). Gliomas are particularly well vascularized and, therefore, serve as a model to study the process of tumor angiogenesis and to investigate anti-angiogenic therapies. Tumor angiogenesis results in vessels with severe malformations. The morphology of the new tumor vessels is dilated, tortuous, elongated, and chaotically organized. Tumor vessels can be void of smooth muscle cells and lack normal innervation (Jain, 2003). Unlike the vessels in normal brain tissue, tumor vessels are highly permeable (Dvorak et al., 1999), allowing the selective uptake of anticancer drugs (Konno et al., 1986).

Identification of reliable models that recapitulate the cellular and molecular features of specific human cancers is needed to accelerate both the understanding of the molecular pathogenesis of cancer and the discovery of therapeutic targets (Peterson et al., 1994). As knowledge of the molecular biology of neoplasia has advanced, transgenic technology has been utilized in elucidating the complex molecular mechanisms underlying oncogenesis and progression of brain tumors. Experimental models for brain tumors that include genetically modified mice, with overexpressed and/or deleted genes, have been created (Ding et al., 2001; Reilly and Jacks, 2001; Hu and Holland, 2005). However, since there are no adequate mechanisms to correlate genetic alterations in mouse tumors with their proposed human counterpart, to what extent the existing mouse models mimic the biology of brain cancer in humans remains uncertain. The gene expression profiles, controlling elements, pathways, and cells of origin for brain tumors remain largely unknown and the molecular elements, such as tissue-specific promoters and enhancers, to create genetically accurate models of brain tumors are still poorly understood. On the other hand, established human glioma cell lines experience over time numerous morphologic and genetic changes and do not reproduce the biology of the tumor in vivo. This study aims to better standardise an orthotopic model of mouse infiltrating astrocytoma that mimics the human clinical situation in terms of histopathological characteristics and angiogenic features.

We have developed a transplant-based model of mouse astrocytoma derived from cultured CT-2A cells (Zimmerman and Arnold, 1941; Abate et al., 2006) which closely replicates the biology of human astrocytoma more efficiently than do the currently available immortalized glioma cell lines and other in vivo models. Characterization of the experimental tumor was performed using histopathology, immuno-histochemistry, and non-invasive imaging procedures (MRI). In conclusion, this tumor model recapitulates well the human astrocytoma disease and can be used for preclinical testing.

Material and methods

Cell culture

CT-2A mouse astrocytoma cells (Abate et al., 2006) were obtained as a generous gift from Prof. T.N. Seyfried (Boston, MA, USA). Tumor cells were grown in RPMI 1640 medium (Gibco, Invitrogen Co., Carlsbad, CA, USA) supplemented with 10% heat-inactivated fetal bovine serum (R10) in a humidified

atmosphere containing 95% air and 5% CO_2 at 37°C. Upon reaching confluency, the cells were trypsinized and collected. The pellet was resuspended in RPMI 1640 medium and the cell suspension was adjusted to obtain an appropriate concentration of cells for injection ($8x10^4$ cells in 4 μl).

Mouse model

A total of forty one adult 12-week-old C57BL/6J, four BALB/c, and four SJL female mice (Harlan Iberica, Barcelona, Spain) weighing 20-25 g were used in this study. All procedures were carried out in accordance with the European Communities Council Directive (86/609/EEE) on animal experiments and with the Ethical Committee of the Spanish Council for Scientific Research (CSIC).

CT-2A cells were injected into the right caudate-putamen (CP) of twenty six experimental animals by intracranial injection using stereotaxic guidance. Mice were deeply anesthetized with pentobarbital (10 mg/kg) and atropine (90 mg/kg) intraperitoneally and placed in a mouse stereotaxic frame (David Kopf Instruments, Tujunga, CA, USA). While under deep anesthesia, a sagittal incision was made through the skin to expose the skull, and a burr hole was drilled at 0.1 mm anterior and 2.25 mm lateral to bregma. A 10 μl Hamilton syringe (Hamilton, Reno, NV, USA) with a 27-gauge needle was inserted at the depth of 2.7 mm from brain surface for infusion of tumor cells. The tumor cells were injected over 15 min. at a speed of 1 μl/3 min. The burr hole was then filled with spongostan (Ferrosan A/S, Soeborg, Denmark) and the scalp sutured. Tumor growth and progression were examined by *in vivo* MRI and histopathology at 7, 14, 21, and 28 days following cell injection. A total of four animals received an intracranial injection of 4 μl of RPMI 1640 medium in the CP. These animals, used as controls, were processed in parallel with those receiving CT-2A cells.

Alternatively, CT-2A tumor cells re-isolated from an *in vivo* experimental CT-2A brain tumor, were injected again in the CP of two healthy anesthetized mice. For this, the experimental CT-2A tumor was excised from the brain, washed with minimal essential medium containing 1% penicillin and streptomycin (Gibco), minced and triturated with a Pasteur pipette while in R10 medium, and plated into plastic culture flasks. At confluency, the cultures were trypsinized, and the pellet resuspended in RPMI 1640 medium. The cell suspension was adjusted to obtain an appropriate concentration of cells for injection ($8x10^4$ cells in 4 μl).

CT-2A cells were also injected in the carotid artery, to simulate metastatic invasion. For this, following alcohol disinfection, the skin of the neck of four C57BL/6J mice was cut by a medial incision, and the common right side carotid artery was exposed. Three ligatures of 7-0 silk suture were placed, i) around the origin of the common carotid artery, ii) proximal to the carotidal bifurcation, which was not closed immediately, and iii) around the origin of the external carotid. A polyethylene tube (PE 10, BD, Franklin Lakes, NJ, USA) containing the tumor cell suspension ($8x10^4$ cells in 10 μl) and connected to a 50 μl Hamilton syringe was inserted into the common carotid artery and placed in the origin of the internal carotid artery. At this point, the second ligature was tightened around the polyethylene tube to avoid leakage. After tube insertion, a volume of 10 μl containing the cell suspension was slowly injected.

The external carotid artery was kept permanently closed to prevent tumor cell reflux into the external carotid and subsequent local tumor cell spread. Then, the tube was removed and the second ligature was closed permanently.

To investigate the influence of the immune system in tumor progression, CT-2A cells were injected in four BALBc and four SJL mice. No tumors developed in these mice.

Magnetic resonance imaging

Mouse tumor growth was imaged weekly by MRI, starting 7 days after tumor cell injection, at 4.7 Teslas using a BIOSPEC BMT 47/40 (Bruker, Ettlingen, Germany), equipped with a 12 cm actively shielded gradient system. Mice were anaesthetized as above and injected intraperitoneally with 0.4 mmol/kg Gadopentetate dimeglumine (Gadolinium, Magnevist, Schering, Germany). Mice were put in prone position inside a cradle to avoid unexpected movements. A respiration sensor was used to survey the animals vital functions. First we acquired T2 weighted images using a fast spin echo sequence. The acquisition parameters were: TR = 4000 ms, effective TE = 60 ms, FOV = 3 cm, Slice Thickness = 1 mm and matrix = 256x192. This matrix size was increased during reconstruction by a zero-filling process in order to obtain images of 256x256 pixels. After that, we acquired T1 (TR/TE=700/15 ms) weighted spin echo images using the same geometrical parameters as above. These images were used to calculate tumor volume using ParaVision software (Bruker, Ettlingen, Germany).

HR-MAS ^{1}H NMR data acquisition

The spectroscopy procedures followed in this study have been previously described (Cheng et al., 1998). Briefly, tissue specimens taken from CT-2A tumor and the contralateral healthy region were snap-frozen in liquid nitrogen and maintained at -80°C until spectroscopic analysis. Cerebral tissue was examined using high resolution magic angle spinning (HR-MAS) operating at 4°C to minimize tissue degradation, 1H-NMR spectroscopy was performed at 500.13 MHz using a Bruker AMX500 spectrometer 11.7 T. Samples were obtained from histologically defined coronal slides of brains four weeks after CT-2A implants and were placed within a 12 ml zirconium oxide rotor with spherical insert and spun at 4000 Hz spinning rate, to remove the

effects of spinning side bands from the spectra acquired. Shimming and NMR preparation time was kept to a minimum and the NMR analysis was performed at 4°C to minimize metabolic changes. Under such conditions no noticeable biochemical degradation of the samples was observed during spectral acquisition. Standard solvent suppressed spectra were acquired in 16 k data points, averaged over 128 acquisitions, total acquisition ~5 min using a sequence based on the first increment of the NOESY pulse sequence to effect suppression of the water resonance and limit the effect of B_o and B_1 in homogeneities in the spectra (relaxation delay-90°-t_1-90°-t_m-90°- acquire free induction decay (FID)) in which a secondary radio frequency irradiation field is applied at the water resonance frequency during the relaxation delay of 1s and during the mixing period (t_m = 150ms), with t_1 fixed at 3 s. A spectral width of 8333.33 Hz was used. All spectra were processed using TOPSPIN software, version 1.3 (Bruker Rheinstetten, Germany). Prior to Fourier transformation, the FIDs were multiplied by an exponential weight function corresponding to a line broadening of 0.3 Hz. Spectra were phased, baseline-corrected and referenced to the sodium TSP [(3-trimethylsilyl)-2,2,3,3-tetradeuteriopropionate] singlet at δ 0ppm. ^{1}H NMR spectra were data reduced using the software program AMIX (Analysis of MIXtures version 3.6.8, Bruker Rheinstetten, Germany) by subdivision into integral regions of 0.02 ppm between δ 0.4 and 4.6 ppm. Individual integral regions were normalized to the total integral region following exclusion of the water resonance. Principal component analysis (PCA) was applied to the data and used no scaling by weighting each integral region or variable by $1/\sqrt{Sk}$ where Sk represents the standard deviation of the variable. The analysis increased the representation of lower concentration metabolites in the resultant data models while minimizing noise. Loading plots from the PCA were used to identify metabolites.

Histopathology

All mice were clinically evaluated and sacrificed at different time intervals, 7, 14, 21, and 28 days following cell implants. Experimental animals were sacrificed if they showed signs of motor disfunction or exhibited symptoms consistent with failure to thrive as per animal care protocols. Histopathology was performed on coronal tissue sections obtained through the same rostro-caudal levels that were previously identified by MRI as exhibiting tumor growth. Mice were deeply anesthetized as for MRI and then perfused transcardially through a blunt cannula with 20 ml phosphate-buffered saline (PBS) followed by 40 ml of 4% paraformaldehyde in 0.1 M phosphate buffer (PB), pH 7.4. Brains were then removed and post-fixed for 4 hours by immersion in the same fixative, at room temperature. For H&E stain tissue blocks were paraffin embedded and then cut coronally in 5-μm sections. For light microscopy immuno-histochemistry, brain tissue was sectioned at 40-μm in the coronal plane with the aid of a vibratome (Leica Microsystems GmbH, Wetzlar, Germany).

Immunohistochemistry

The expression of the p53 tumor suppressor protein (p53) in the experimental tumor was evaluated using a mouse monoclonal antibody (EXBIO, Praha, Czech Republic). The glial origin of the CT-2A cells was indicated by the presence of GFAP by using a mouse monoclonal antibody (GFAP, Sigma CO, St. Louis, MO, USA). The presence of Sox family of transcription factors 9 and 10 in tumor cells was screened by using polyclonal antibodies which have been previously characterized (Maka et al., 2005; Stolt et al., 2003) and were a generous gift from Dr. Michael Wegner (Institut fur Biochimie, Universitat Erlangen-Nuremberg, Germany). Polyclonal antibodies against NOS isoforms (neuronal: nNOS, endothelial: eNOS, and inducible: iNOS) and nitrotyrosine, a marker of final protein nitration (Encinas et al., 2003), were used to follow the expression of the nitrergic system as the experimental CT-2A tumor grew. Antisera against nNOS, iNOS and nitrotyrosine were produced in house as previously described (Rodrigo et al., 1994). eNOS immuno-cytochemistry was performed with a polyclonal antibody (Transduction Laboratories, Lexington, KY, USA). Adrenomedullin (AM) expression in CT-2A experimental tumor was carried out by using polyclonal antibodies that were also produced in house (Martinez et al., 1995).

Immunohistochemistry was performed according to standard avidin-biotin-peroxidase complex (ABC) methods (Hsu et al., 1981). Immunohistochemistry with p53 was performed on paraffin-embedded tissue sections (5 μm-thick). For this, tissue sections were pretreated for antigen retrieval at high temperature (microwave) in 10 mM citrate buffer pH 6.0 for 5 min. Immuno-histochemistry for GFAP, Sox transcription factors 9 and 10, NOS isoforms, nitrotyrosine, and AM was carried out in free-floating sections that were preincubated in 1% H_2O_2 in PBS for one hour to block endogenous peroxidase. Sections were then treated with 3% normal serum obtained from the species providing the secondary antibodies diluted in PBS containing 0.2% Triton X-100, for 1 h at room temperature (RT). Then, sections were incubated overnight at 4°C in the primary antibodies diluted in PBS containing 0.2% Triton X-100. Antibodies dilutions were: i) p53, 1:100, ii) GFAP, 1:500; iii) Sox9, 1:2000, iv) Sox10,1:500, v) nNOS, 1:3000), vi) iNOS, 1:5000, vii) eNOS, 1:1000, viii) nitrotyrosine, 1:1000, and ix) AM, 1:1000. After washing thoroughly in PBS, histological sections were incubated with biotinylated secondary antibodies, goat anti-mouse or goat anti-rabbit immunoglobulins 1:200 in PBS (Vector Laboratories, Burlingame, CA, USA), for 1 h at RT. After additional washes, sections were incubated with peroxidase-linked ABC (Vector Laboratories) for 90 min. Peroxidase activity was

developed by nickel enhanced 3,3'-diaminobenzidine tetrahydrochloride (DAB) as described (Rodrigo et al., 1994). Finally, sections were washed, mounted and dehydrated for light microscopy visualization. Histological sections were examined with a Zeiss Axiophot II microscope (Zeiss Iberica, Madrid, Spain) and images captured with a digital camera (DMC le, Polaroid, Cambridge, MA, USA). Immunofluorescence staining for confocal microscopy was carried out by incubating tissue sections in the specific antibodies for GFAP and Sox9 diluted as for ABC procedure. Sections were then thoroughly washed and incubated with Cy3-donkey anti-mouse IgG and Rhodamine Red donkey anti-rabbit IgG (Jackson ImmunoResearch, West Grove PA, USA) diluted 1:200 in PBS, for 1 hour at RT. Confocal images were acquired using a Leica TCS SP5 (Leica Microsystems GmbH, Wetzlar, Germany) scanner.

Ultrastructural studies of experimental CT-2A tumor were carried out in 40-μm-thick tissue sections. Before cutting, tissue blocks were rapidly frozen in liquid nitrogen and thawed in cold 0.1M PB to improve antibody penetration. For the subcellular location of AM, tissue sections were processed as for light microscopy, except that Triton X-100 was avoided in the incubation steps. The immunocytochemical reaction was developed by incubating the tissue sections in PBS containing 0.006% DAB, for 10 min followed by 0.003% of H_2O_2 in the same solution. Subsequently, the sections were washed for 5 min in PBS and PB, postfixed in 1% osmium tetroxide in 0.1M PB for 1 hour, dehydrated in ethanol of increasing concentrations and block-stained in uranyl acetate (1% in 70% ethanol) in the dark for 40 min at room temperature. The sections were then flat embedded and mounted on Durcupan ACM resin slides (Sigma-Aldrich Inc.) under plastic coverslips and cured for 3 days at 56°C. Selected areas of the immunostained tumor were dissected out and re-embedded in Durcupan. Ultrathin sections were obtained with the aid of a Reichert OM U3 ultramicrotome (Reichert, Germany), mounted on formwar-coated grids, stained with lead citrate, and examined under a Jeol 1200 electron microscope (Jeol, Tokyo, Japan) at 80 Kv. No immunolabeling was detected when the primary antibodies were omitted or replaced with an equivalent concentration of normal mouse or rabbit serum. In addition, preabsorption with an excess of the antigen prevented staining in all cases.

Results

Tumor growth

CT-2A cells grew *in vitro* as a monolayer of fusiform shaped cells. Three to four weeks following cell implant, a highly angiogenic and haemorrhagic soft tumor (Fig. 1A) was detected in treated mice, obtaining a 100% tumorigenesis rate. The tumor margins were typically well defined (Fig. 1B-E), merging discernibly with the adjacent white and gray matter (Figs 1E). Five to ten days following intracranial injection with CT-2A cells, a soft, non cohesive hypercellular mass was observed near the injection site (Fig. 1F). Histological analysis showed characteristic features of a high-grade astrocytoma, such as high mitotic index, microvascular proliferation, cellular density and a central area of necrosis (pseudopalisading necrosis) (Figs 1G,H, 2, 3A). The tumors showed extensive heterogeneity (Fig. 1H). A subset of tumor cells infiltrated into the surrounding brain tissue following tracks marked by blood vessels (Fig. 2).

Tumor CT-2A cells harvested from transplanted animals and grown in tissue culture formed a monolayer of fusiform cells. Almost all the cells retrieved from the tumor had morphological characteristics of tumor cells with very little contamination from stromal components, possibly due to the well defined margins of the tumor. These re-cultured tumor cells maintained high proliferating capacity when re-implanted transcranially into healthy mice. In addition, injection of CT-2A cells into the carotid artery caused a metastatic tumor growth in the homolateral hemisphere 7-10 days following cell inoculation in all animals treated. The resulting tumors had the same growing characteristics and histological features as those generated following intracranial CT-2A cell injection (data not shown).

Under the electron microscope, tumor cells were pleomorphic, either large fusiform or small, with characteristic nuclei which exhibited areas of heterochromatin and frequent prominent nucleoli (Fig. 3). The cytoplasm contained abundant mitochondria and polyribosomes, indicating a high metabolic and synthetic rate.

RMI analysis

Conventional T2- and T1- weighted (pre- and Gadolinium post-contrast) MRI images provided exceptional sensitivity in detecting and delineating the location of intracranial tumors (Figs 1B-D, 4). The recognition of intracranial tumors was markedly enhanced with prior administration of Gadolinium (Figs 1B-D; 4A,C,E), with a resolution limit of 0.013 mm^2. T1-weighted imaging with Gadolinium enhancement of vascularity was routinely used to detect tumor location, margins, size, and growth. The MRI images regarding tumor size and location correlated accurately with the results of the histopathological analysis in this study (compare Fig. 1D with Fig. 1E). T1-weighed images revealed a well-defined heterogeneously enhancing mass that arose in the CP (Fig. 1B), extending over time rostro-caudally and eventually involving the cerebral cortex and hippocampus (Figs. 1C,D, 4A,C,E). Occasionally, the tumor grew outside of the skull through the needle tract (Fig. 1C). Tumor progression was verified by serial MRI over time and weekly images of experimental CT-2A tumors were successfully obtained (Fig. 4). The experimental tumor was

characterized by rapid growth being already apparent at 1 week post-injection (Figs. 1B, 4A) and becoming too large at 4 weeks (Figs 1C,D, 4E,F). At that time mice began to present neurological complications and had to be sacrificed for welfare reasons.

Tumor growth resulted in marked deformation of the

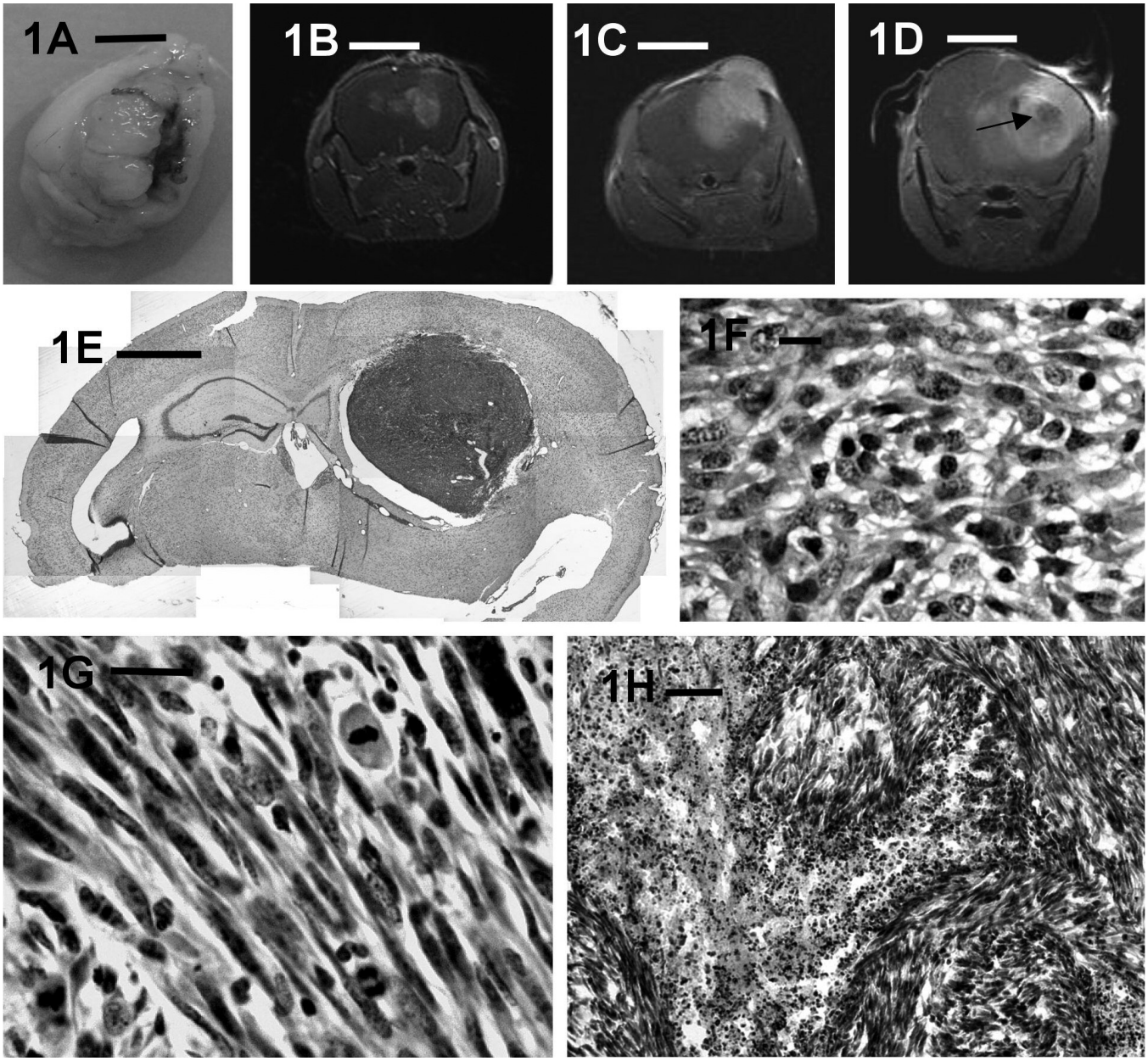

Fig. 1. Characterization of CT-2A induced brain tumors. **A.** Mouse brain with haemorrhagic CT-2A tumor mass lying in the right cerebral hemisphere, 28 days following CT-2A cell injection. The photograph was taken after *in vivo* MRI (**B-D**) and removal of the brain at the time of necropsy for histology (**E, G, H**). **B-D.** T1–weighted (Gadolinium postcontrast) images corresponding to the same experimental CT-2A tumor depicted in A, showing the tumor progression over time, (**B**) one week and (**C, D**) four weeks following cell implant. Notice that in B the hyperintense signal is restricted to the CP on the right hemisphere. **C and D.** Serial coronal MRI images at different distances from the olfactory bulb. The rapid growth of the tumor can be visualized comparing **B with C and D.** Notice that necrosis in **D** appears as an area of decreased T1 signal (arrow). Also, notice in **D** hyperintense signal in the rim of the tumor indicating that the tumor border is well-vascularized. **F.** Histopathologic section through a tumor mass ten days after intracranial CT-2A cell injection. H&E staining revealed high density of irregularly shaped cells. **G, H.** Histopathologic sections of the tumor shown in **B-E** exhibiting the features of GBM following H&E staining, including **(G)** nuclear pleomorfism and numerous mitotic figures and **(H)**, pseudopalidasing, intratumoral hemorrhage and necrosis. Scale bars: A, G, 10 μm; B-E, 5 mm; F, 1.25 mm; H, 20 μm.

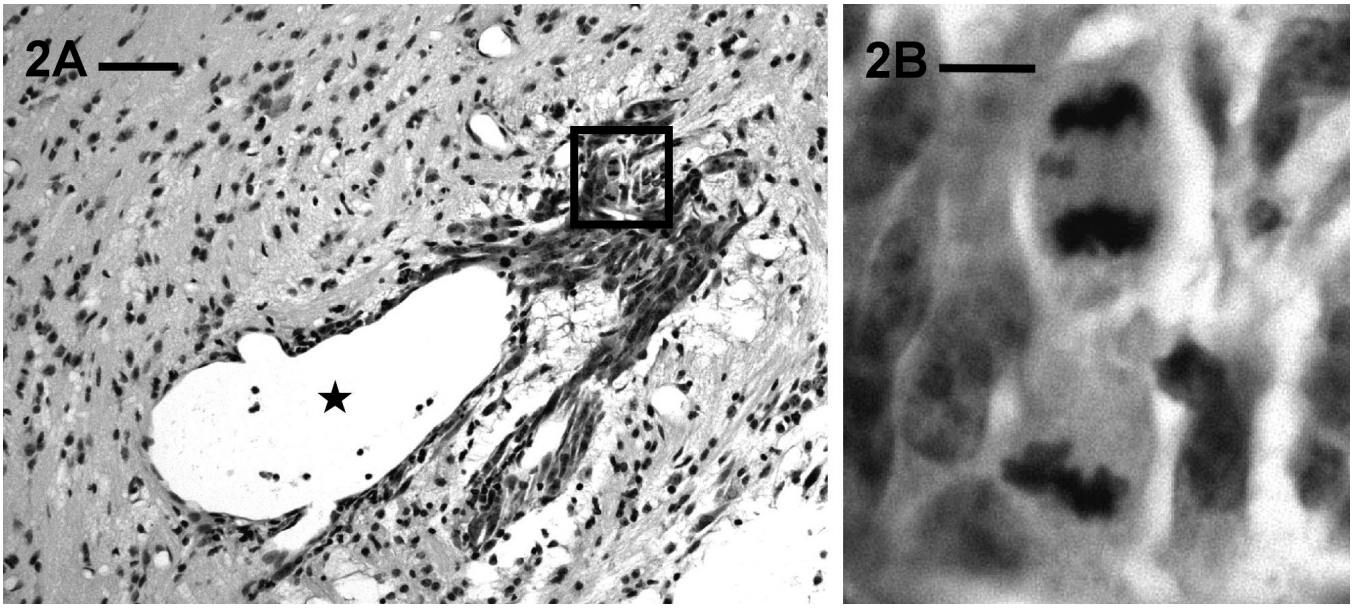

Fig. 2. A. Light micrograph of a H&E stained section illustrating CT-2A cells located close to the rim of the tumor and infiltrating the surrounding neuropil following host vasculature (asterisk) caming from the neighbouring cerebral cortex. **B.** High-power magnification of the boxed area in **A**. Mitotic figures near a pre-existing blood vessel are detected. Scale bars: A, 100 μm; B 10 μm.

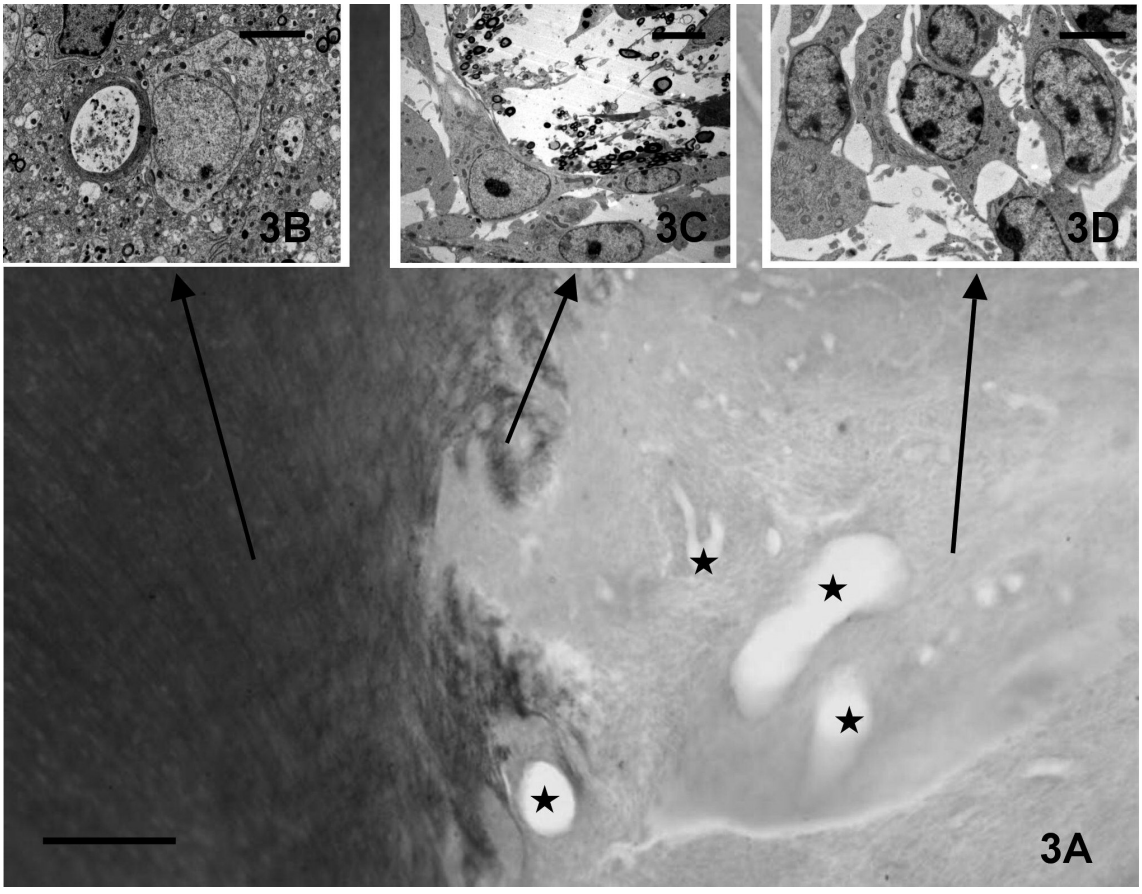

Fig. 3. A. Light micoscopic image of osmium-stained normal brain tissue (dark) and adjacent CT-2A tumor (light color). Numerous intratumoral blood vessels (asterisks) are seen in the tumor. **B.** Electron micrograph showing the fine morphology of the neuropil in normal brain tissue far from tumor growth. **C and D.** Electron micrographs illustrating the ultrastructural appearance of tumor cells in the transition zone **(C)** and deep in the tumor **(D)**. Tumor cells show cytological pleomorphism with prominent nucleoli, slender processes and characteristic heterochromatin. Scale bars: A, 100 μm; B-D, 2.5 μm.

lateral and dorsal third ventricles (Fig. 4D,F). A central hypo-attenuation of the tumor was frequently seen in T1-weighted images suggesting central necrosis (Fig. 1D) which was confirmed in the histological analysis of those cases (Fig. 1G,H). In addition, cystic changes within the tumor were occasionally detected in T2-weighted images (Fig. 4F).Tumor growth provoked signs of destruction of brain parenchyma and of increasing pressure within the brain as it invaded the neighboring brain structures (Figs 1A-E,G,H; 4). After 15-20 days post implantation, mice began to show signs of raised intracranial pressure. Symptoms such as lethargy or motor disfunctions with hunched posture, poor grooming, failure to thrive and weight loss, were common. The periphery of the tumor had in all instances a well-established blood supply as revealed by the enhanced pattern in T1-weighted images with Gadolinium (Fig. 4E).

Immunohistochemistry

Immunostaining for p53 was exclusively nuclear and was exhibited by numerous cells in the tumor mass (Fig. 5A). GFAP immunoreactivity was detected in normal astrocytes of the brain parenchyma outside the tumor and also in tumor cells (Fig. 5B-E). The reaction product

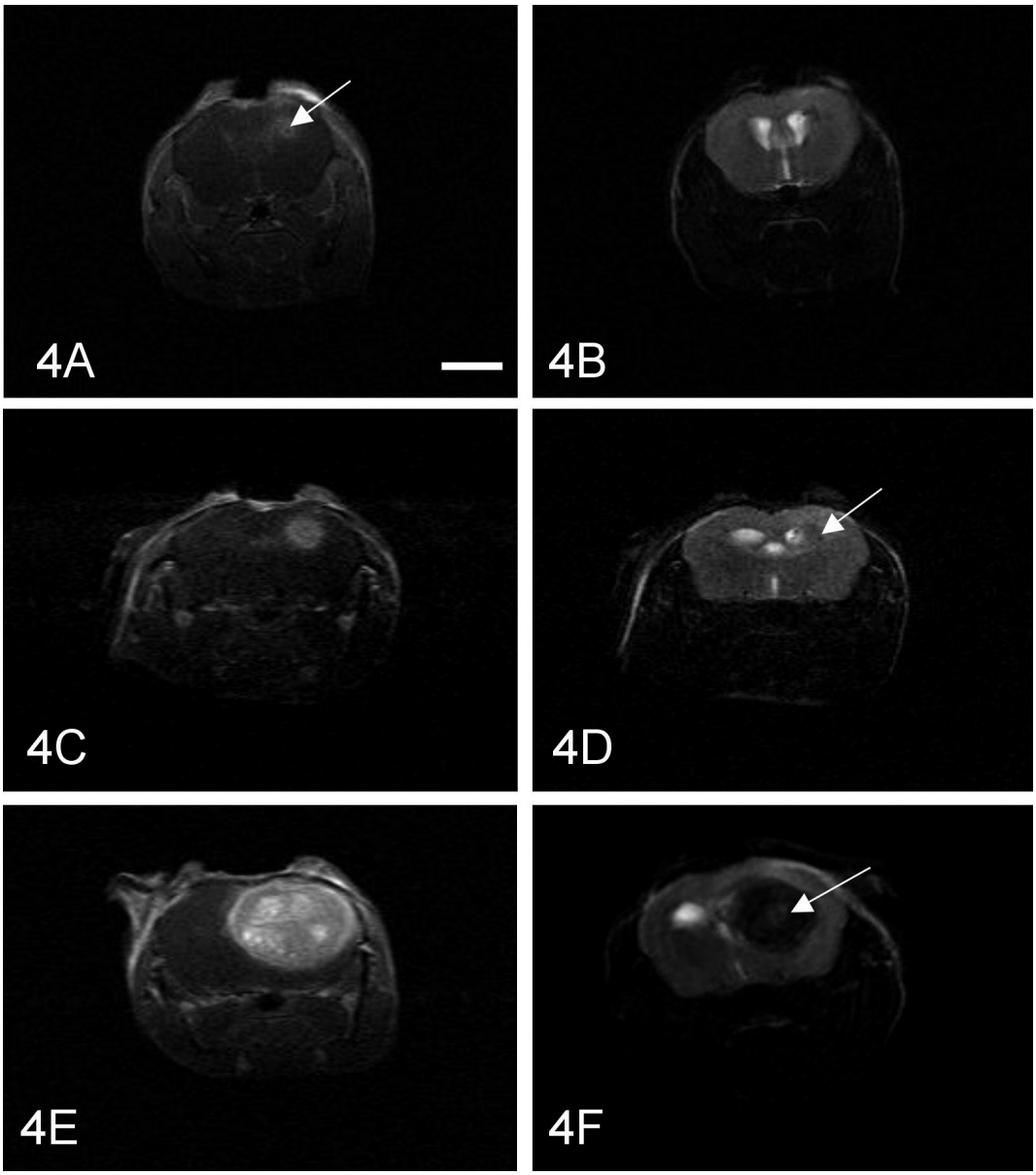

Fig. 4. MRI coronal images performed at different time intervals showing progressive tumor growth in an experimental animal after intracranial injection of CT-2A astrocytoma cells. Assessment of tumor volume changes is shown by using Gadolinium enhanced T1- (**A, C, E**) and T2- (**B, D, F**) weighted images. A,B, Sections at the same level one week post injection. A small tumor mass in **A** (arrow) is located deep in the CP. At this time point, T2-weighted image (**B**) is unable to detect the tumor mass shown in A. **C, D.** Aspect of the tumor two weeks post-injection. At this time point, the tumor mass (arrow in **D**) displaces the lateral ventricle allowing tumor identification by T2-weighted image. **E, F.** Enlarged tumor four weeks post-injection. Thin rim of contrast enhancement is seen around the tumor as well as a nodular enhancement inside the tumor **(E)**. With T2 a mass effect distorting the right lateral and dorsal ventricles and a small enhancing hyperintense area (arrow) likely representing a cyst are clearly seen **(F)**. Scale bar: 5 μm.

accumulated diffusely in the cytoplasm of tumor cells, and GFAP-positive cells were more frequent in the tumor edge (Fig. 5E). GFAP immunostaining also delineated the wall of small vessels within the tumor (Fig. 5C). Characteristically, astrocytes showing normal features (Fig. 5D) were not detected inside the tumor where only tumor cells were positive for GFAP (Fig. 5E).

Sox9 and Sox10 immunocytochemical expressions presented different patterns in experimental CT-2A tumors. Tumor cells displaying strong nuclear staining for either Sox9 or Sox10 were detected in the tumor cells and in normal astrocytes (Fig. 6). Numerous Sox9 positive cells were detected within the tumor mass, being more abundant near blood vessels and in the tumor rim (Fig. 6A,B). Immunoreactive Sox10 cells in the rim of the tumor were also abundant (Fig. 6C,D). In contrast, Sox10 immunoreactive cells were very infrequent inside the tumor mass. Double immunofluorescence revealed that Sox9- and GFAP-positive CT-2A cells formed distinct subpopulations (Fig. 6E). CT-2A cells exhibiting both Sox9- and GFAP-positive staining were numerous, but cells staining for only one of the antibodies were also located (Fig. 6E). As expected, astrocytes in the

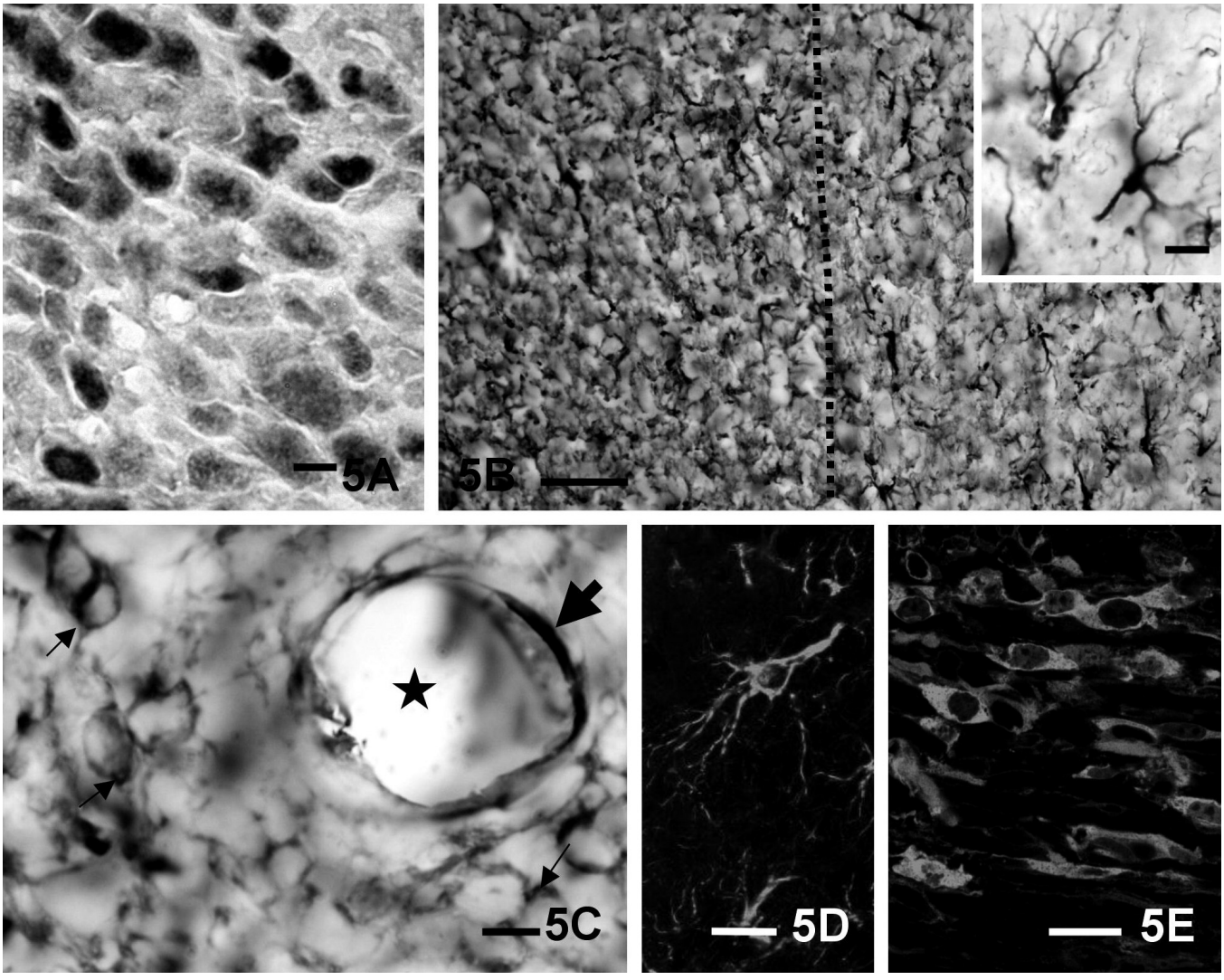

Fig. 5. A. Immunocytochemical staining of p53 in a CT-2A tumor mass showing nuclear staining. **B-E.** GFAP-positive structures in and around the experimental tumor as revealed by immunohistochemistry **(B, C)** and immunofluorescence **(D, E)** staining procedures. **B.** Distribution of the immunoreaction product in both normal brain tissue (right hand side) and the CT-2A tumor (left hand side). Inset in **A** is a high-power magnification photograph showing two immunoreactive astrocytes in the normal neuropil surrounding the tumor. **C.** High-power magnification of the tumor area showing the elevated cell density of GFAP-positive tumor cells (some pointed by arrows) and the presence of immunostaining (thick arrow) in the wall of a capillary (asterisk). **D, E.** GFAP-positivity in astrocytes near tumor mass **(D)** and in CT-2A cells **(E)**. Scale bars: A: 10 μm; B, 100 μm; C-E, inset in B, 20 μm.

neocortex exhibited double labelling for GFAP and Sox9 (Fig. 6F). Remarkably, we also observed Sox9 positive staining in Golgi-like structures of GFAP-negative cells, probably belonging to cortical neurons (arrows in Fig. 6F).

With regard to the immunocytochemical location of

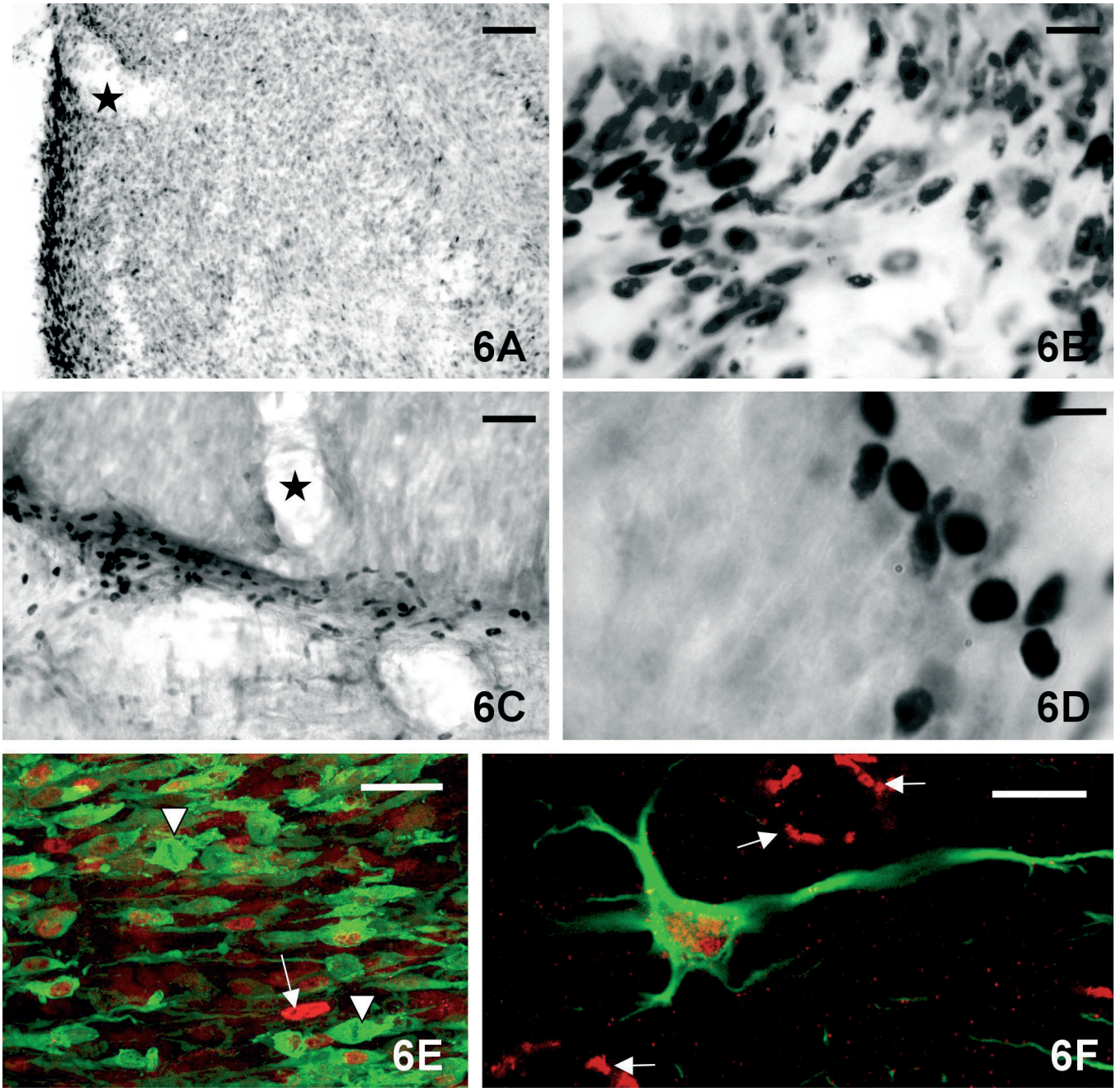

Fig. 6. Distribution of Sox9 (**A, B, E, F**) and Sox10 (**C, D**) in and around the experimental tumor. **A.** High cellular density of Sox9 stained cells was seen near blood vessels (asterisk) and in the rim of the tumor. **B.** is a higher-power magnification micrograph of stained structures shown in **A**. **C.** Sox10-positive cells accumulated in the rim of the tumor. **D.** Details of immunoreactive cells displayed in **C**. Both immunoreactivities were located in the cell nuclei (**E, D**). Note in **A** and **C** the rich vasculature (asterisks) in the rim of the tumor. **E, F.** Double immunofluorescence staining of a section through the tumor mass (**E**) and the cerebral cortex (**F**) double labelled for GFAP (green) and Sox9 (red). Most tumor cells stained for both GFAP and Sox9, although a few cells expressed GFAP and not Sox9 (arrowheads) or viceversa (arrow). In normal brain (**F**), astrocytes express both. Surprisingly, Sox9 staining was also found in structures suggesting Golgi apparatus cisternae of neighboring GFAP-negative cells (some pointed by arrows). Scale bars: A, C, E, 100 μm; B, 20 μm; D, F, G, 10 μm; H, 30 μm.

the nitrergic system, we found that nNOS staining revealed a complete destruction of the nNOS neuronal network within the tumor (Fig. 7A). Positive nNOS neurons exhibiting varicose processes suggesting advanced neurodegeneration were often detected in the margins of the tumor (Fig. 7A,B), whereas no nNOS immunoreactive cell was seen further inside the tumor. In the neuropil outside the tumor, nNOS immunoreaction product marked neurons showing normal morphologies (Fig. 7A,C). The complete

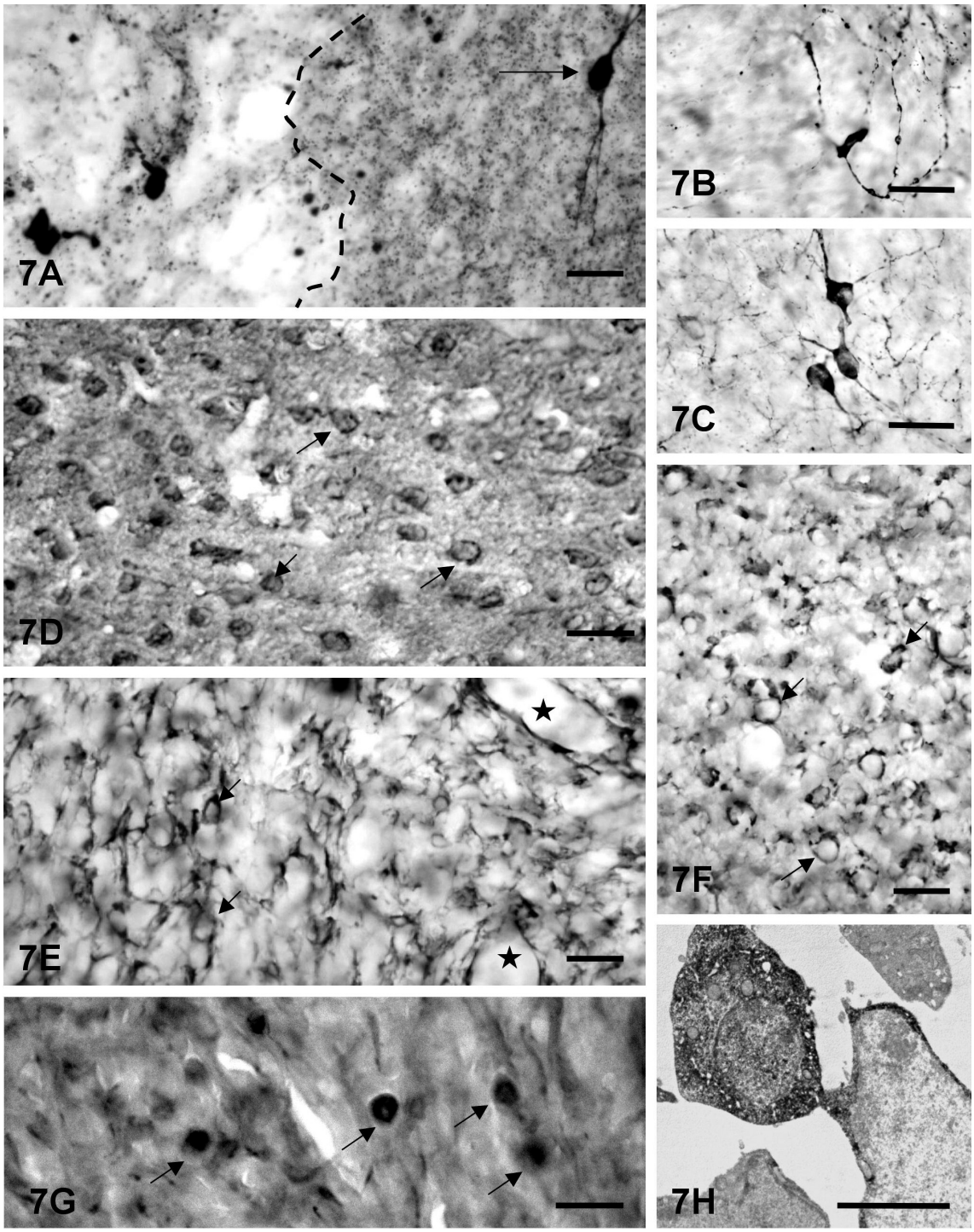

Fig. 7. Immunocytochemical localization of nNOS (**A-C**), iNOS (**D**), eNOS (**E**), nitrotyrosine (**F**) and AM (**G, H**) in the experimental CT-2A tumor. Left-hand side in **A** and **B**, nNOS-positive neurons in the tumor mass exhibiting abnormal features. Notice in **A** and **B** that immunoreactive neurons in the tumor mass display varicose processes suggesting degeneration. In contrast, an nNOS immunoreactive neuron showing typical morphology can be appreciated in the CP (arrow) near the tumor mass (**A**). **C.** nNOS-positive neurons in the side contralateral to the tumor displaying typical morphology. A number of tumor cells (some pointed by arrows) are seen exhibiting immunostaining for iNOS particularly in the rim of the tumor (**D**), eNOS (**E**), nitrotyrosine (**F**) and AM (**G**). **E.** Depicts immunoreaction product associated to the wall of small capillaries (asterisks). **H.** Illustrates intense immunostaining in tumor cells characteristically showing cytological pleomorphism by electron microscopy. Scale bars: A-C, 20 μm; D-G, 10 μm; H, 2 μm.

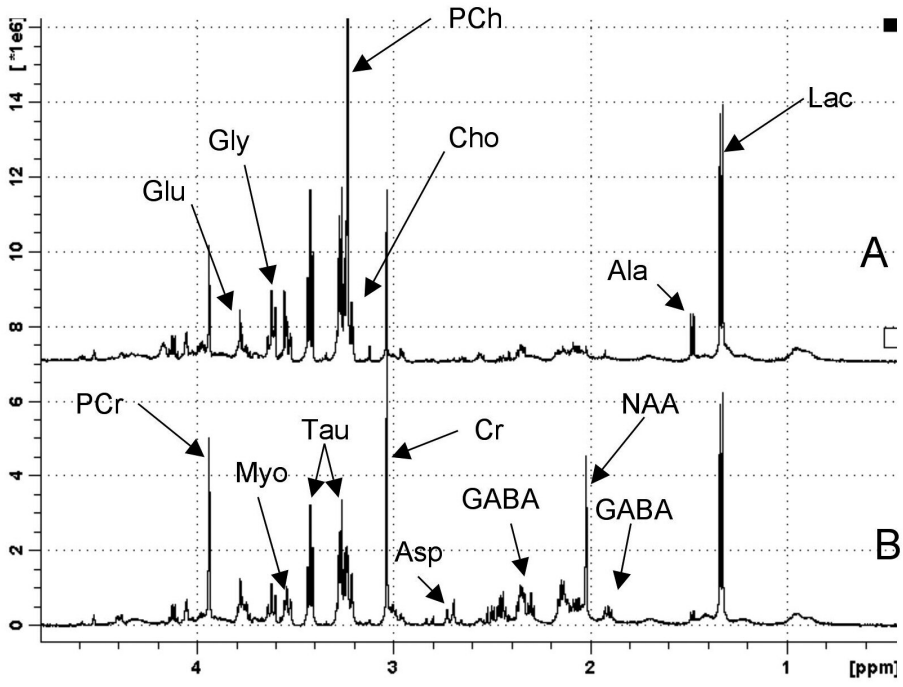

Fig. 8. High-resolution ^{1}H-NMR spectra of aqueous extracts of CT-2A tumor **(A)** and of the normal contralateral area **(B)**. Selected metabolite resonances are labelled on spectrum. Abbreviations in the figure correspond to: Ala: alanine; Asp: aspartate; Cho: choline; Cr: creatine; GABA: γ-aminobutyric acid; Glu: glutamate; Gly: glycine; Lac: lactate; Myo: myoinositol; NAA: N-acetylaspartate; PCh: phosphorylcholine; PCr: phosphocreatine; Tau: taurine

degeneration of the neuronal network was also seen by electron microscopy (Fig. 3). In contrast, iNOS, eNOS, and nitrotyrosine immunoreactivities were stronger in tumor structures than in the surrounding brain tissue (Fig.7D-F). iNOS, eNOS, and nitrotyrosine immunoreactivities typically labeled the cytoplasm of a subset of tumor cells (Fig. 7D,E,F). In addition, eNOS staining was very intense in the wall of blood vessels (Fig. 7E). Outside the tumor, eNOS was detected in endothelia of blood vessels and occasional astrocyte-like cells, but never in neurons (data not shown). No immunoreactivity for either iNOS or nitrotyrosine was seen in the non-affected neuropil.

Concerning AM immunoreactivity, light and electron microscopic studies revealed deposition of the reaction product in the cell nucleus and/or cytoplasm of a subpopulation of tumor cells (Fig. 7G,H). Through the electron microscope, these cells show the immunoreaction product associated with the external surface of cytoplasmatic organelles and the cell nucleus and the inner surface of the cytoplasmatic membrane (Fig. 7H). AM immunoreactive cells lie in the proximity of non-immunoreactive tumor cells showing similar morphological traits. Positive and negative tumor cells were pleomorphic, with either large fusiform or small rounded morphology.

HR-MAS ^{1}H NMR

A direct comparison between the ex vivo HR-MAS ^{1}H NMR spectra of the CT-2A tumor and normal brain in the contralateral side of the tumor, was carried out using both comparison of metabolite ratios and/or pattern recognition methods (Fig. 8). Spectra were composed of resonances deriving, among others, from lactate (Lac), alanine (Ala), γ-aminobutyric acid (GABA), acetate (Ace), glutamate (Glu), aspartate (Asp), creatine (Cr), choline (Cho), phosphorylcholine (PCh), taurine (Tau), N-acetylaspartate (NAA) myo-inositol (Myo), and glycine (Gly). Following the same criteria used by Tsang et al. (2005) we found no significant biochemical degradation of the samples during spectral acquisition. The spectrum of the CT-2A tumor, compared with the normal contralateral brain, revealed an increased signal for Cho (at 3.20 ppm), and PCh (at 3.22 ppm). There were also higher signals in the tumor related with Lac (at 1.3 ppm), Ala (at 1.48 ppm), Tau (at 3.26 ppm and 3.42 ppm), Gly (at 3.56 ppm), Myo (at 3.53) and Glu (at 3.79 ppm). On the other hand, the tumor showed lower signals for NAA (at 2.02 ppm), GABA (at 1.83 ppm and 2.22 ppm), Asp (at 2.68-2.82 ppm), and Cr (at 3.04 ppm).

Discussion

We have standardized an orthotopic mouse model of malignant mouse astrocytoma, CT-2A, in terms of histopathological characteristics and angiogenic features. The animal model has been produced after an intracerebral injection of CT-2A cells (Seyfried et al., 1992) into the CP. The resulting CT-2A tumor model exhibited common features with the human astrocytoma disease, as shown by histopathology, immunohisto-chemistry, and non-invasive imaging procedures (MRI).

Given that tumor-host interactions are organ specific, mouse models should be orthotopic to better reproduce their biology. It is also important to take into account the contribution of the immune system. For this reason our model was developed using immunocompetent syngeneic mice.

CT-2A tumor cells were produced in the Seyfried laboratory by implantation of a chemical carcinogen, 20-methylcholanthrene, into the cerebral cortex of C57BL/6J mice, following previous descriptions (Zimmerman and Arnold, 1941). By implanting CT-2A tumor pieces (about 1 mm^3) from donor mice into the cerebral cortex of C57BL/6J mice, a syngeneic mouse brain tumor model was produced (Seyfried et al., 1992; Abate et al., 2006). Our procedure initiating tumors from cultured CT-2A cells instead of from solid tumors improved the method by using a determined number of cells to initiate the tumor, providing a more quantitative approach when studying the effect of various treatments on tumor growth. Additionally, we kept brain damage to a minimum due to tumor implantation by injecting a liquid cell suspension rather than tissue fragments. Intracranial xenograft mouse models using tumor cell lines or primary cultures have been reported previously in immunodeficient mice (Bock et al., 2003; Singh et al., 2004).

The injection of the CT-2A cells into the CP produced an aggressive astrocytic neoplasm histopathologically characterized by pleomorphic, hyperproliferative, and infiltrative cells. Our observation that the CT-2A experimental tumor exhibits the characteristics of a poorly differentiated malignant astrocytoma is consistent with previous reports (Seyfried et al., 1992; Mukherjee et al., 2002, 2004). Over time, tumors became highly cellular with frequent mitosis and other pathologic characteristics, including vascular proliferation and areas of necrosis with pseudopalisading tumor cells, characterizing them as GBM (Yates, 1992; Fischer et al., 2005; Rong et al., 2006).

In addition to malignant mouse CT-2A model, other astrocytoma models have been available both *in vitro* and *in vivo* (Ding et al., 2001; Reilly and Jacks, 2001; Hu and Holland, 2005; King et al., 2005; Kang et al., 2006; Khain and Sander, 2006; Lee et al., 2006; Terzis et al., 2006). However, many of the available models used to study gliomas in mice and rats do not correctly reproduce all of the important characteristics of malignant gliomas in humans, including variability of phenotypes within individual tumors, the migratory characteristics *in vivo* that are such an important feature of human CNS tumors and the appearance of radioresistance and chemoresistance. In addition, established human glioma cell lines develop multiple genetic changes over time, so that they may no longer reflect the biology of the tumor in the patient. Consequently, implantation of these cells in experimental animals will not reproduce the interaction between tumor and host that occurs in humans. Tumor heterogeneity introduces a further difficulty in the identification of the best-fit mouse models for human cancers.

Metastases of tumor cells of various origins to the brain are frequent (Reilly and Jacks, 2001; Kirsch and Loeffler, 2004; Becher et al., 2006). To find out whether CT-2A cells may provide a valid model for brain metastasis, these cells were injected in the internal carotid artery and metastatic tumor growths were found in the brain parenchyma, ipsilateral to the injection site. This demonstrates also that the progression of the tumor occurs independently of the lesion caused by the needle during the injection protocol. Additionally, CT-2A cells re-isolated from experimental CT-2A tumors, and later injected into the CP, generated new tumors identical to the original tumor. Together, these data provide direct evidence that experimental CT-2A tumors contain cancerous initiating cells. These cells have potent in vivo self-renewal and proliferative capacities, generating tumors that are a phenocopy of the primary experimental tumor. These facts suggest the existence of tumor stem cells among the CT-2A cells but a formal identification of these stem cells should be carried out. In human GBM, CD133+ cells have been identified and proposed as potential tumor stem cells (Singh et al., 2004).

Injection of CT-2A cells in mouse strains other than C57BL/6J did not produce any tumor growth, even 3 months after implantation. CT-2A cells were generated in C57BL/6J mice (Zimmerman and Arnold, 1941) and, obviously, are able to escape the immune surveillance in this strain but not in others.

To further characterize the phenotype of the CT-2A induced tumors, detailed immunohistochemical analyses were performed. Immunohistochemical examination showed strong positivity for GFAP, the different NOS isoforms, nitrotyrosine, AM, Sox9, and Sox10.

The observation of endogenous GFAP in tumor cells correlates well with previous descriptions that tumor cells in human astrocytomas express GFAP (Schiffer et al., 1986; Sembritzki et al., 2002). The morphology of the GFAP-positive cells inside the tumor is clearly neoplastic and rather different from normal astrocytes in the undisturbed parenchyma, indicating that they were derived from the CT-2A cells and were not trapped normal astrocytes, which seem to be utterly destroyed by the tumor as happens with the neurons.

Both in normal and pathological situations, NO plays various functions in the CNS including vasodilatation, neurotransmission, neural plasticity, neurotoxicity, and oxidative stress (Rodrigo et al., 2005). Malignant brain neoplasms express high levels of NOS suggesting that NO production may be associated with pathophysiological processes essential to these tumors (Broholm et al., 2003). Although the biological role of NO in malignancies is still poorly understood, recent investigations suggest that it may have a dual pro- and anti-tumor action. While NO can inhibit cell growth and initiate a free radical injury to normal and tumor cells leading to apoptosis and necrosis (Tews, 1999), it can stimulate cell growth, dilate the vessels surrounding the

tumor thereby ensuring supply, and induce tumor angiogenesis (Lam-Himlin et al., 2006). It has also been proposed that NO might stimulate tumor growth and metastasis by promoting migration, invasion, and angiogenesis (Pan et al., 2005). NO production in the endothelium of the intratumoral blood vessels has been associated with blood flow regulation of the tumor and as a possible cause of brain edema (Broholm et al., 2003). Overexpression of eNOS in astrocytoma plays a crucial role in tumor angiogenesis (Pan et al., 2005). Taken together, these findings suggest that modulation of NO production may provide a new therapeutic approach for brain cancers (Morbidelli et al., 2004; Pan et al., 2005; Lam-Himlin et al., 2006).

We found that cancer cells characteristically did not express nNOS and, in fact, the lack of nNOS immunoreactivity perfectly demarcated the tumor boundaries. A small number of nNOS immunoreactive neurons were detected in the periphery of tumor surrounded by tumor cells. These cells were swollen and exhibited processes with abnormal dilatations in their course, suggesting advanced neurodegeneration. It is well known that excessive NO generation during stroke, ischemia, and neurodegenerative diseases contributes to neuronal cell death (Coyle and Puttfarcken, 1993; Dawson and Dawson, 1996). In clear contrast, expression of iNOS was only found in the tumor and not in the surrounding parenchyma. Our results correlate with previous findings in humans showing expression of iNOS immunoreactivity only in proliferative tumor cells (Kao et al., 2003). We also found a strong staining for eNOS in both tumor cells and blood vessels, whereas only a faint immunoreaction was seen in normal vessels in unaffected areas. This has also been found in human GBM (Pan et al., 2005). Since progressive tumor growth is dependent on angiogenesis, the strong expression of eNOS immunoreactivity within the tumor suggests that the angiogenic switch has been pushed towards active angiogenesis promotion. The intense staining for iNOS and eNOS inside the tumor suggests that excessive NO may be produced at the tumor site. This is also supported by the presence of nitrated proteins as shown by nitrotyrosine immunoreactivity. This excessive production of NO may be responsible for the destruction of the brain parenchyma.

AM is a multifunctional regulatory peptide (Lopez and Martinez, 2002) that operates as a growth factor for tumor cells, reduces apoptosis, augments tumor cell motility, and increases angiogenesis (Martinez et al., 2002). In the CNS, AM is produced by a variety of cells, including neurons and astrocytes (Serrano et al., 2000). The expression of AM peptide and its receptor in human gliomas has been previously reported (Benes et al., 2004; Mennel et al., 2006). Our identification of a subpopulation of CT-2A tumor cells exhibiting AM immunoreactivity correlates well with these previous findings and supports previous studies that AM may function as an autocrine growth factor for glioblastoma cells (Ouafik et al., 2002; Boudouresque et al., 2005). AM is highly induced *in vitro* by hypoxia in human T98G glioblastoma cells (Kitamuro et al., 2000) through a HIF-1 mediated mechanism (Garayoa et al., 2000). It has been demonstrated that the use of specific antibodies against AM consistently reduces the growth of established glioblastoma xenografts through angiogenesis supression (Ouafik et al., 2002). Following this line of research, we have proceeded to evaluate in vivo the action of the antiangiogenic small molecule 77427 (Martinez et al., 2005; Martinez, 2006) in CT-2A tumor growth. The results of this experiment are still very preliminary but they show a reduction of the tumor volume over time. Since 77427 was applied systemically, our preliminary results indicate either that 77427 can cross the blood-brain barrier or that the tumor vasculature allows the extravasation of this small molecule. In either case, 77427 may constitute a promising new drug for the treatment of brain cancers.

Sox (Sry-type HMG box) genes constitute a large family of transcription factors that play critical roles in gene regulation during embryogenesis (Wegner, 2001). These proteins belong to the High Mobility Group (HMG) superfamily, which is well conserved across species. Neural crest development is regulated by the transcription factor Sox9 (Cheung and Briscoe, 2003) which is strongly expressed first in neural stem cells and then in glial cells of the CNS, which suggests Sox9 as a component of the mechanism that causes neural stem cells to switch from neurogenesis to gliogenesis (Stolt et al., 2003). Levels of HMG protein expression have been correlated with tumor progression, with malignant cells expressing high levels and benign tumor cells or normal cells in adult tissues exhibiting little or no expression of Sox9 (Wunderlich and Bottger, 1997). It has been suggested that Sox9 suppresses apoptosis (Akiyama et al., 2002), and this protein has been proposed as a novel candidate marker of stem cells (Sottile et al., 2006) and a potential genetic marker for cancer (Dong et al., 2004). In the CNS, Sox10 transcripts were originally thought to be confined to glial precursors but later were detected in oligodendrocytes of the adult brain, being considered one of the main determinants of oligodendroglial differentiation (Stolt et al., 2002). Although a high number of astrocytomas express Sox10 (Bannykh et al., 2006), such expression occurs at lower levels. In connection with these reports, our findings demonstrated Sox9 immunostaining in a large number of tumor cells, but only a few cells expressed Sox10 immunoreactivity. This observation suggests that experimental CT-2A tumors might contain at least two chemically, and perhaps functionally, distinct cell subpopulations. However, the fact that tumor cells may modify antigenic expressions during cell cycle should be taken into account. Interestingly, we observed that not every GFAP positive tumor cell expressed Sox9. This finding correlates with the fact that in adult rodent brain Sox9 immunoreactivity colocalizes only partially (40%) with astrocytes (Pompolo and Harley, 2001). The observation of intense nuclear staining for Sox9 in our experimental

tumor cells coincides with the same observation in high grade tumors in humans (Dong et al., 2004; Bannykh et al., 2006; Kordes and Hagel, 2006). The results of this study reinforce the connection between Sox gene expression and astrocytic tumors.

Tumor angiogenesis was evaluated in the CT-2A experimental model both histologically and by contrast enhanced MRI with gadolinium. Imaging plays a major role in current cancer detection and treatment. Monitoring techniques such as in vivo MRI allow for evaluation studies of the validity of the model employed, providing quantitative aspects of tumor biology, such as growth kinetics, vascularity, and cellularity. Standard T1- and T2-weighted MRI identify brain tumors with high sensitivity. As in humans, the use of contrast-enhanced MRI in mice with brain tumors provided in vivo anatomical information on the cerebral tumor as to its precise localization and extent. Besides primary information on the size and localization of the tumor, MRI also provides information on secondary phenomena such as mass effect, edema, hemorrhage, necrosis, and signs of increased intracranial pressure at high spatial resolution and with high tissue contrast (Koutcher et al., 2002).

Although MRI can be very helpful for identifying pathologic abnormalities, it has limitations when evaluating gliomas (Floeth and Stummer, 2005; Dyke et al., 2007) and histologic confirmation is necessary to establish an accurate diagnosis. Normally, higher-grade tumors frequently show enhancement on MRI, but enhancement does not always equate with histologic tumor grade. The HR-MAS 1H NMR application is actually extensively applied to human tissues because it correlates more closely with histologic findings and provides a powerful tool for assessing tumor presence and extent (Balmaceda et al., 2006; Hollingworth et al., 2006; Omuro et al., 2006). Metabolite levels measured with HR-MAS 1H NMR can be consistently correlated with tumor types and grades and the monitoring of progression of pathology in human brain (Li et al., 2004; Dyke et al., 2007). In our study, HR-MAS ^{1}H NMR spectroscopy revealed distinct differences in the metabolic tissue profile in CT-2A tumors compared with normal contralateral parenchyma. These changes, which showed a close relationship with previous findings in human GBM (Li et al., 2004; Oh et al., 2004; Balmaceda et al., 2006; Dyke et al., 2007), included a predominant signal at 3.2 ppm and 3.22 ppm, attributed to Cho-containing compounds, associated with low intensity peaks at 3.04 ppm, attributable to Cr derivatives. Human rapidly growing neoplasms show the common feature of an increased Cho/Cr ratio, a decreased NAA/Cr ratio, and an increased Lac/ Cr level (Li et al., 2004; Dyke et al., 2007). The high Cho-containing compounds/Cr ratio found has been linked with synthesis of new cell membranes and increased membrane turnover and higher cellular density (Floeth and Stummer, 2005; Tugnoli et al., 2005). Interestingly, it has also been proved that human pathological samples with increased Lac/Cr ratio exhibited characteristic features of necrosis (Son et al., 2001). The presence of elevated Cho and decreased Ace has been found to correlate with tumor histologic findings and may be used in distinguishing regions of possible cancer from normal and other noncancerous tissue, including necrosis and astrogliosis (Dowling et al., 2001). Higher levels of Lac have been attributed to hypoxia and the grade of malignancy of the tumor and are usually detected in GBM (Castillo et al., 1996; Dyke et al., 2007). Elevated Lac levels in CT-2A tumor probably imply greater glucose and glycogen levels in this region. Low signal at 2.02 attributable to NAA was observed in CT-2A tumors, suggesting that a decrease in brain NAA concentrations correlates directly with histopathological evidence of neuronal loss in CT-2A tumor as previously reported (Cheng et al., 1997). High signals at 3.63 ppm (Myo), 3.56 ppm (Gly) and 3.26-3.42 ppm (Tau) were observed in CT-2A tumors. The elevation of Myo and Tau is related to the hypothesis that Myo is a glial marker and that Tau is synthesized from cysteine by astrocytes but not by primary neurons (Brand et al., 1993). Both *in vivo* and *in vitro* NMR spectroscopy studies demonstrated that Myo, Gly, and Tau concentrations were correlated with cell density in tumors. The quantification of tumor metabolic changes with HR-MAS, in conjunction with subsequent histopathology of the same tumor specimen, has the potential to further our knowledge on the biochemistry of CT-2A tumor heterogeneity during progression, and ultimately to improve our accuracy in diagnosing, characterizing, and evaluating tumor progression for preclinical trials.

In summary, orthotopic tumors produced by the injection of CT-2A cells in the CP of C57BL/6J mice closely resemble human GBM tumors and may be a good model for preclinical trials of novel anticancer drugs for CNS malignancies.

Acknowledgements: This study was supported by grants from the Spanish Ministry for Science and Education, BFU2004/02838, and SAF2005/02608, and the CSIC/Community of Madrid, 200620M001. We gratefully acknowledge Prof. T.N. Seyfried (Biology Department, Boston College, MA) for the gift of the CT-2A cells and Prof. Michael Wegner (Institut fur Biochimie, Universitat Erlangen-Nuremberg, Germany) for the Sox9 and Sox10 antibodies. We are very grateful for the excellent technical assistance of Ms. Africa Sandonis.

References

Abate L.E., Mukherjee P. and Seyfried T.N. (2006). Gene-linked shift in ganglioside distribution influences growth and vascularity in a mouse astrocytoma. J. Neurochem. 98, 1973-1984.

Akiyama H., Chaboissier M.C., Martin J.F., Schedl A. and de Crombrugghe B. (2002). The transcription factor Sox9 has essential roles in successive steps of the chondrocyte differentiation pathway and is required for expression of Sox5 and Sox6. Genes Dev. 16, 2813-2828.

Balmaceda C., Critchell D., Mao X., Cheung K., Pannullo S., DeLaPaz

R.L. and Shungu D.C. (2006). Multisection 1H magnetic resonance spectroscopic imaging assessment of glioma response to chemotherapy. J. Neurooncol. 76, 185-191.

Bannykh S.I., Stolt C.C., Kim J., Perry A. and Wegner M. (2006). Oligodendroglial-specific transcriptional factor SOX10 is ubiquitously expressed in human gliomas. J. Neurooncol. 76, 115-127.

Becher M.W., Abel T.W., Thompson R.C., Weaver K.D., and Davis L.E. (2006). Immunohistochemical analysis of metastatic neoplasms of the central nervous system. J. Neuropathol. Exp. Neurol. 65, 935-944.

Benes L., Kappus C., McGregor G.P., Bertalanffy H., Mennel H.D. and Hagner S. (2004). The immunohistochemical expression of calcitonin receptor-like receptor (CRLR) in human gliomas. J. Clin. Pathol. 57, 172-176.

Bock N.A., Zadeh G., Davidson L.M., Qian B., Sled J.G., Guha A. and Henkelman R.M. (2003). High-resolution longitudinal screening with magnetic resonance imaging in a murine brain cancer model. Neoplasia 5, 546-554.

Boudouresque F., Berthois Y., Martin P.M., Figarella-Branger D., Chinot O. and Ouafik L. (2005). [Role of adrenomedullin in glioblastomas growth]. Bull. Cancer 92, 317-326.

Brand A., Richter-Landsberg C., and Leibfritz D. (1993). Multinuclear NMR studies on the energy metabolism of glial and neuronal cells. Dev. Neurosci. 15, 289-298.

Broholm H., Rubin I., Kruse A., Braendstrup O., Schmidt K., Skriver E.B. and Lauritzen M. (2003). Nitric oxide synthase expression and enzymatic activity in human brain tumors. Clin. Neuropathol. 22, 273-281.

Brown J.M. and Wilson W.R. (2004). Exploiting tumour hypoxia in cancer treatment. Nat. Rev. Cancer 4, 437-447.

Castillo M., Kwock L. and Mukherji S.K. (1996). Clinical applications of proton MR spectroscopy. AJNR Am. J. Neuroradiol. 17, 1-15.

CBTRUS (2005). Statistical report: Primary brain tumors in the United States, 1998-2002. Published by the Central Brain Tumor Registry of the United States.

Cheng L.L., Chang I.W., Louis D.N. and Gonzalez R.G. (1998). Correlation of high-resolution magic angle spinning proton magnetic resonance spectroscopy with histopathology of intact human brain tumor specimens. Cancer Res. 58, 1825-1832.

Cheng L.L., Ma M.J., Becerra L., Ptak T., Tracey I., Lackner A. and Gonzalez R.G. (1997). Quantitative neuropathology by high resolution magic angle spinning proton magnetic resonance spectroscopy. Proc. Natl. Acad. Sci. USA 94, 6408-6413.

Cheung M. and Briscoe J. (2003). Neural crest development is regulated by the transcription factor Sox9. Development 130, 5681-5693.

Coyle J.T. and Puttfarcken P. (1993). Oxidative stress, glutamate, and neurodegenerative disorders. Science 262, 689-695.

Dawson V.L. and Dawson T.M. (1996). Nitric oxide neurotoxicity. J. Chem. Neuroanat. 10, 179-190.

DeAngelis L.M. (2001). Brain tumors. N. Engl. J. Med. 344, 114-123.

Deorah S., Lynch C.F., Sibenaller Z.A. and Ryken T.C. (2006). Trends in brain cancer incidence and survival in the United States: Surveillance, Epidemiology, and End Results Program, 1973 to 2001. Neurosurg. Focus. 20, E1.

Ding H., Roncari L., Shannon P., Wu X., Lau N., Karaskova J., Gutmann D.H., Squire J.A., Nagy A. and Guha A. (2001). Astrocyte-specific expression of activated p21-ras results in malignant astrocytoma formation in a transgenic mouse model of human gliomas. Cancer Res. 61, 3826-3836.

Dong C., Wilhelm D. and Koopman P. (2004). Sox genes and cancer. Cytogenet. Genome Res. 105, 442-447.

Dowling C., Bollen A.W., Noworolski S.M., McDermott M.W., Barbaro N.M., Day M.R., Henry R.G., Chang S.M., Dillon W.P., Nelson S.J. and Vigneron D.B. (2001). Preoperative proton MR spectroscopic imaging of brain tumors: correlation with histopathologic analysis of resection specimens. AJNR Am. J. Neuroradiol. 22, 604-612.

Dvorak H.F., Nagy J.A., Feng D., Brown L.F. and Dvorak A.M. (1999). Vascular permeability factor/vascular endothelial growth factor and the significance of microvascular hyperpermeability in angiogenesis. Curr. Top. Microbiol. Immunol. 237, 97-132.

Dyke J.P., Sanelli P.C., Voss H.U., Serventi J.V., Stieg P.E., Schwartz T.H., Ballon D., Shungu D.C. and Pannullo S.C. (2007). Monitoring the effects of BCNU chemotherapy Wafers (Gliadel((R))) in glioblastoma multiforme with proton magnetic resonance spectroscopic imaging at 3.0 Tesla. J. Neurooncol. 82, 103-110.

Encinas J.M., Serrano J., Bentura M.L., Castro-Blanco S., Fernandez A.P. and Rodrigo J. (2003). Nitric oxide system and protein nitration are modified by an acute hypobaric hypoxia in the adult rat hippocampus. J. Neuropathol. Exp. Neurol. 62, 863-877.

Fan X., Salford L.G., and Widegren B. (2006). Glioma stem cells: Evidence and limitation. Semin. Cancer Biol. 17, 214-218.

Fischer I., Gagner J.P., Law M., Newcomb E.W. and Zagzag D. (2005). Angiogenesis in gliomas: biology and molecular pathophysiology. Brain Pathol. 15, 297-310.

Floeth F.W. and Stummer W. (2005). The value of metabolic imaging in diagnosis and resection of cerebral gliomas. Nat. Clin. Pract. Neurol. 1, 62-63.

Folkman J. (1971). Tumor angiogenesis: therapeutic implications. N. Engl. J. Med. 285, 1182-1186.

Folkman J. (1992). The role of angiogenesis in tumor growth. Semin. Cancer Biol. 3, 65-71.

Garayoa M., Martinez A., Lee S., Pio R., An W.G., Neckers L., Trepel J., Montuenga L.M., Ryan H., Johnson R., Gassmann M. and Cuttitta F. (2000). Hypoxia-inducible factor-1 (HIF-1) up-regulates adrenomedullin expression in human tumor cell lines during oxygen deprivation: a possible promotion mechanism of carcinogenesis. Mol. Endocrinol. 14, 848-862.

Gasparini G., Longo R., Toi M. and Ferrara N. (2005). Angiogenic inhibitors: a new therapeutic strategy in oncology. Nat. Clin. Pract. Oncol. 2, 562-577.

Hanahan D. and Folkman J. (1996). Patterns and emerging mechanisms of the angiogenic switch during tumorigenesis. Cell 86, 353-364.

Hollingworth W., Medina L.S., Lenkinski R.E., Shibata D.K., Bernal B., Zurakowski D., Comstock B. and Jarvik J.G. (2006). A systematic literature review of magnetic resonance spectroscopy for the characterization of brain tumors. AJNR Am. J. Neuroradiol. 27, 1404-1411.

Holmgren L., O'Reilly M.S., and Folkman J. (1995). Dormancy of micrometastases: balanced proliferation and apoptosis in the presence of angiogenesis suppression. Nat. Med. 1, 149-153.

Hsu S.M., Raine L. and Fanger H. (1981). Use of avidin-biotin-peroxidase complex (ABC) in immunoperoxidase techniques: a comparison between ABC and unlabeled antibody (PAP) procedures. J. Histochem. Cytochem. 29, 577-580.

Hu X. and Holland E.C. (2005). Applications of mouse glioma models in preclinical trials. Mutat. Res. 576, 54-65.

Jain R.K. (2003). Molecular regulation of vessel maturation. Nat. Med. 9, 685-693.

Jung C.R., Hwang K.S., Yoo J., Cho W.K., Kim J.M., Kim W.H., and Im D.S. (2006). E2-EPF UCP targets pVHL for degradation and associates with tumor growth and metastasis. Nat. Med. 12, 809-816.

Kaiser J. (1999). No meeting of minds on childhood cancer. Science 286, 1832-1834.

Kalluri R. and Zeisberg M. (2006). Fibroblasts in cancer. Nat. Rev. Cancer 6, 392-401.

Kang S.H., Cho H.T., Devi S., Zhang Z., Escuin D., Liang Z., Mao H., Brat D.J., Olson J.J., Simons J.W., Lavallee T.M., Giannakakou P., Van Meir E.G. and Shim H. (2006). Antitumor effect of 2-methoxyestradiol in a rat orthotopic brain tumor model. Cancer Res. 66, 11991-11997.

Kao C.L., Chiou S.H., Chen H.S., Ho D.M., Chen C.F., Ho L.L., Lee M.J. and Wong T.T. (2003). Elevated nitric oxide levels in childhood brain tumors. Childs Nerv. Syst. 19, 744-749.

Kaur B., Tan C., Brat D.J., Post D.E. and Van Meir E.G. (2004). Genetic and hypoxic regulation of angiogenesis in gliomas. J. Neurooncol. 70, 229-243.

Khain E. and Sander L.M. (2006). Dynamics and pattern formation in invasive tumor growth. Phys. Rev. Lett. 96, 188103.

King G.D., Curtin J.F., Candolfi M., Kroeger K., Lowenstein P.R. and Castro M.G. (2005). Gene therapy and targeted toxins for glioma. Curr. Gene Ther. 5, 535-557.

Kirsch D.G. and Loeffler J.S. (2004). Treating brain metastases: current approaches and future directions. Expert. Rev. Neurother. 4, 1015-1022.

Kitamuro T., Takahashi K., Nakayama M., Murakami O., Hida W., Shirato K. and Shibahara S. (2000). Induction of adrenomedullin during hypoxia in cultured human glioblastoma cells. J. Neurochem. 75, 1826-1833.

Kleihues P., Louis D.N., Scheithauer B.W., Rorke L.B., Reifenberger G., Burger P.C. and Cavenee W.K. (2002). The WHO classification of tumors of the nervous system. J. Neuropathol. Exp. Neurol. 61, 215-225.

Kleihues P. and Ohgaki H. (1997). Genetics of glioma progression and the definition of primary and secondary glioblastoma. Brain Pathol. 7, 1131-1136.

Konno T., Ohtsuka N., Yamasaki K., Mizutani J., Miyauchi Y., Maeda H. and Matsumura Y. (1986). [Targeting of anticancer chemotherapy utilizing the characteristic nature of the neovasculature of solid tumors]. Gan To Kagaku Ryoho. 13, 1448-1455.

Kordes U. and Hagel C. (2006). Expression of SOX9 and SOX10 in central neuroepithelial tumor: Hamburg, 07.04.2006. J. Neurooncol. 80, 151-155.

Koutcher J.A., Hu X., Xu S., Gade T.P., Leeds N., Zhou X.J., Zagzag D. and Holland E.C. (2002). MRI of mouse models for gliomas shows similarities to humans and can be used to identify mice for preclinical trials. Neoplasia 4, 480-485.

Lam-Himlin D., Espey M.G., Perry G., Smith M.A. and Castellani R.J. (2006). Malignant glioma progression and nitric oxide. Neurochem. Int. 49, 764-768.

Lee J., Kotliarova S., Kotliarov Y., Li A., Su Q., Donin N.M., Pastorino S., Purow B.W., Christopher N., Zhang W., Park J.K. and Fine H.A. (2006). Tumor stem cells derived from glioblastomas cultured in bFGF and EGF more closely mirror the phenotype and genotype of primary tumors than do serum-cultured cell lines. Cancer Cell 9, 391-403.

Li X., Jin H., Lu Y., Oh J., Chang S. and Nelson S.J. (2004). Identification of MRI and 1H MRSI parameters that may predict survival for patients with malignant gliomas. NMR Biomed. 17, 10-20.

Lopez J. and Martinez A. (2002). Cell and molecular biology of the multifunctional peptide, adrenomedullin. Int. Rev. Cytol. 221, 1-92.

Maka M., Stolt C.C. and Wegner M. (2005). Identification of Sox8 as a modifier gene in a mouse model of Hirschsprung disease reveals underlying molecular defect. Dev. Biol. 277, 155-169.

Martinez A. (2006). A new family of angiogenic factors. Cancer Lett. 236, 157-163.

Martinez A., Miller M.J., Unsworth E.J., Siegfried J.M. and Cuttitta F. (1995). Expression of adrenomedullin in normal human lung and in pulmonary tumors. Endocrinology 136, 4099-4105.

Martinez A., Vos M., Guedez L., Kaur G., Chen Z., Garayoa M., Pio R., Moody T., Stetler-Stevenson W.G., Kleinman H.K. and Cuttitta F. (2002). The effects of adrenomedullin overexpression in breast tumor cells. J. Natl. Cancer Inst. 94, 1226-1237.

Martinez A., Zudaire E., Julian M., Moody T.W. and Cuttitta F. (2005). Gastrin-releasing peptide (GRP) induces angiogenesis and the specific GRP blocker 77427 inhibits tumor growth in vitro and in vivo. Oncogene 24, 4106-4113.

McKinley B.P., Michalek A.M., Fenstermaker R.A. and Plunkett R.J. (2000). The impact of age and sex on the incidence of glial tumors in New York state from 1976 to 1995. J. Neurosurg. 93, 932-939.

Mennel H.D., Hallier-Neelsen M., Hagner S. and Benes L. (2006). Two novel cell specific receptor proteins, CRLR and CD 117 in human glial tumors. Clin. Neuropathol. 25, 107-114.

Morbidelli L., Donnini S. and Ziche M. (2004). Role of nitric oxide in tumor angiogenesis. Cancer Treat. Res. 117, 155-167.

Mukherjee P., Abate L.E. and Seyfried T.N. (2004). Antiangiogenic and proapoptotic effects of dietary restriction on experimental mouse and human brain tumors. Clin. Cancer Res. 10, 5622-5629.

Mukherjee P., El-Abbadi M.M., Kasperzyk J.L., Ranes M.K. and Seyfried T.N. (2002). Dietary restriction reduces angiogenesis and growth in an orthotopic mouse brain tumour model. Br. J. Cancer 86, 1615-1621.

Oh J., Henry R.G., Pirzkall A., Lu Y., Li X., Catalaa I., Chang S., Dillon W.P. and Nelson S.J. (2004). Survival analysis in patients with glioblastoma multiforme: predictive value of choline-to-N-acetylaspartate index, apparent diffusion coefficient, and relative cerebral blood volume. J. Magn Reson. Imaging 19, 546-554.

Omuro A.M., Leite C.C., Mokhtari K. and Delattre J.Y. (2006). Pitfalls in the diagnosis of brain tumours. Lancet Neurol. 5, 937-948.

Ouafik L., Sauze S., Boudouresque F., Chinot O., Delfino C., Fina F., Vuaroqueaux V., Dussert C., Palmari J., Dufour H., Grisoli F., Casellas P., Brunner N. and Martin P.M. (2002). Neutralization of adrenomedullin inhibits the growth of human glioblastoma cell lines in vitro and suppresses tumor xenograft growth in vivo. Am. J. Pathol. 160, 1279-1292.

Pan J.W., Zhan R.Y., Tong Y., Zhou Y.Q. and Zhang M. (2005). Expression of endothelial nitric oxide synthase and vascular endothelial growth factor in association with neovascularization in human primary astrocytoma. J. Zhejiang. Univ. Sci. B. 6, 693-698.

Patel N.S., Li J.L., Generali D., Poulsom R., Cranston D.W. and Harris A.L. (2005). Up-regulation of delta-like 4 ligand in human tumor vasculature and the role of basal expression in endothelial cell function. Cancer Res. 65, 8690-8697.

Peterson D.L., Sheridan P.J. and Brown W.E. Jr (1994). Animal models for brain tumors: historical perspectives and future directions. J. Neurosurg. 80, 865-876.

Pompolo S. and Harley V.R. (2001). Localisation of the SRY-related HMG box protein, SOX9, in rodent brain. Brain Res. 906, 143-148.

Reilly K.M. and Jacks T. (2001). Genetically engineered mouse models of astrocytoma: GEMs in the rough? Semin. Cancer Biol. 11, 177-191.

Rodrigo J., Springall D.R., Uttenthal O., Bentura M.L., Abadia-Molina F., Riveros-Moreno V., Martinez-Murillo R., Polak J.M. and Moncada S. (1994). Localization of nitric oxide synthase in the adult rat brain. Philos. Trans. R. Soc. Lond B Biol. Sci. 345, 175-221.

Rodrigo J., Fernandez A.P., Serrano J., Peinado M.A., and Martinez A. (2005). The role of free radicals in cerebral hypoxia and ischemia. Free Radic. Biol. Med. 39, 26-50.

Rong Y., Durden D.L., Van Meir E.G. and Brat D.J. (2006). 'Pseudopalisading' necrosis in glioblastoma: a familiar morphologic feature that links vascular pathology, hypoxia, and angiogenesis. J. Neuropathol. Exp. Neurol. 65, 529-539.

Schiffer D., Giordana M.T., Germano I. and Mauro A. (1986). Anaplasia and heterogeneity of GFAP expression in gliomas. Tumori 72, 163-170.

Sembritzki O., Hagel C., Lamszus K., Deppert W. and Bohn W. (2002). Cytoplasmic localization of wild-type p53 in glioblastomas correlates with expression of vimentin and glial fibrillary acidic protein. Neurooncol. 4, 171-178.

Serrano J., Uttenthal L.O., Martinez A., Fernandez A.P., Martinez D.V., Alonso D., Bentura M.L., Santacana M., Gallardo J.R., Martinez-Murillo R., Cuttitta F. and Rodrigo J. (2000). Distribution of adrenomedullin-like immunoreactivity in the rat central nervous system by light and electron microscopy. Brain Res. 853, 245-268.

Seyfried T.N., el-Abbadi M. and Roy M.L. (1992). Ganglioside distribution in murine neural tumors. Mol. Chem. Neuropathol. 17, 147-167.

Singh S.K., Hawkins C., Clarke I.D., Squire J.A., Bayani J., Hide T., Henkelman R.M., Cusimano M.D. and Dirks P.B. (2004). Identification of human brain tumour initiating cells. Nature 432, 396-401.

Son B.C., Kim M.C., Choi B.G., Kim E.N., Baik H.M., Choe B.Y., Naruse S. and Kang J.K. (2001). Proton magnetic resonance chemical shift imaging (1H CSI)-directed stereotactic biopsy. Acta Neurochir. (Wien.). 143, 45-49.

Sottile V., Li M. and Scotting P.J. (2006). Stem cell marker expression in the Bergmann glia population of the adult mouse brain. Brain Res. 1099, 8-17.

Stolt C.C., Rehberg S., Ader M., Lommes P., Riethmacher D., Schachner M., Bartsch U. and Wegner M. (2002). Terminal differentiation of myelin-forming oligodendrocytes depends on the transcription factor Sox10. Genes Dev. 16, 165-170.

Stolt C.C., Lommes P., Sock E., Chaboissier M.C., Schedl A. and Wegner M. (2003). The Sox9 transcription factor determines glial fate choice in the developing spinal cord. Genes Dev. 17, 1677-1689.

Terzis A.J., Niclou S.P., Rajcevic U., Danzeisen C. and Bjerkvig R. (2006). Cell therapies for glioblastoma. Expert. Opin. Biol. Ther. 6, 739-749.

Tews D.S. (1999). Cell death and oxidative stress in gliomas. Neuropathol. Appl. Neurobiol. 25, 272-284.

Tsang T.M., Griffin J.L., Haselden J., Fish C. and Holmes E. (2005). Metabolic characterization of distinct neuroanatomical regions in rats by magic angle spinning 1H nuclear magnetic resonance spectroscopy. Magn. Reson. Med. 53, 1018-1024.

Tugnoli V., Schenetti L., Mucci A., Nocetti L., Toraci C., Mavilla L., Basso G., Rovati R., Tavani F., Zunarelli E., Righi V. and Tosi M.R. (2005). A comparison between in vivo and ex vivo HR-MAS 1H MR spectra of a pediatric posterior fossa lesion. Int. J. Mol. Med. 16, 301-307.

Vescovi A.L., Galli R. and Reynolds B.A. (2006). Brain tumour stem cells. Nat. Rev. Cancer. 6, 425-436.

Wegner M. (2001). Expression of transcription factors during oligodendroglial development. Microsc. Res. Tech. 52, 746-752.

Wesseling P., van der Laak J.A., Link M., Teepen H.L. and Ruiter D.J. (1998). Quantitative analysis of microvascular changes in diffuse astrocytic neoplasms with increasing grade of malignancy. Hum. Pathol. 29, 352-358.

Wunderlich V. and Bottger M. (1997). High-mobility-group proteins and cancer--an emerging link. J. Cancer Res. Clin. Oncol. 123, 133-140.

Yates A.J. (1992). An overview of principles for classifying brain tumors. Mol. Chem. Neuropathol. 17, 103-120.

Zimmerman H. and Arnold H. (1941). Experimental brain tumors. I. Tumors produced with methylcholantrene. Cancer Res. 1, 919-938.

Accepted May 23, 2007